Collision Detection for Low-Cost Robot Manipulators Using Probabilistic Residual Torque Modeling

Yifei Simon Shao[1,2], Baljeet Singh[1], Nicholas Morozovsky[1], and Pengkang Yu[1]

***Abstract*— With the advancement of robot manipulator technologies, developing custom-made low-cost manipulator arms has gained increasing popularity in the field of robotics. However, these low-cost systems often lack precise sensing and control capabilities, making reliable collision detection particularly critical to ensure safe operation. Popular methods of collision detection, which estimate external disturbances such as generalized Momentum Observer (MO) critically rely on an accurate dynamics model, and precise system identification requires joint torque sensors that are expensive for low-cost manipulators. This paper presents a novel approach to improve collision detection for low-cost robot manipulators where modeling error is present and torque sensing is not available. We propose a probabilistic framework using Gaussian Mixture Models (GMM) to capture friction and other unmodeled dynamics of a robot manipulator. Instead of explicitly identifying model parameters, GMM is created on the total residual torque of the MO while running an excitation trajectory. The GMM is then deployed in the main control loop to identify external disturbances from the residual torque of the same momentum observer. The approach is validated on a custom-made 4-Degrees-of-Freedom (DoF) robot arm with modeling error, unmodeled dynamics, and with only joint position measurement. Our method achieves reliable detection on both hard and soft collisions, demonstrating a reduction in the false positive rate by more than 50% compared to conventional MO-based methods with the same true positive rate on the same hardware.**

I. INTRODUCTION

Safe physical human-robot interaction and reliable manipulation tasks fundamentally depend on effective collision detection capabilities [1]. Collision detection methods based on only proprioceptive sensors are preferred for their reliability and faster response. Over the past decades, numerous collision detection methods have been developed, and their performance is validated with experiments on commercial robot manipulators [2], [3]. Unlike the high-end commercial manipulators, the rising popularity of custom-made, low-cost robot manipulators presents unique challenges in this domain. These challenges stem from the inherent limitations of low-cost hardware and the more pronounced manufacturing imperfections associated with low-cost components.

As established in robotics literature, collision monitoring and detection are the two initial phases in the collision event pipeline for robot manipulators [2]. Conventional collision monitoring approaches, particularly those based on observers, rely heavily on either accurate torque measurements or accurate dynamics models [4], especially when detecting soft and light collisions. However, such accuracy is difficult to achieve in low-cost systems. Obtaining precise torque measurements is challenging, because joint torque sensors are expensive and are often omitted to reduce costs. Instead, these systems typically estimate joint torque through motor current measurements, which introduces significant uncertainties due to inaccurate motor torque constant and complicated friction characteristics. In terms of the requirement of accurate dynamics models, conventional system identification techniques require direct force and torque measurements, accurate acceleration measurements, and elaborate calibration procedures, making them impractical for low-cost applications [5]. Recent research has investigated data-driven and machine learning approaches to capture system dynamics, detailed in Section II. However, these methods either demand substantial computational resources to train models, or still require joint acceleration or torque measurements for training and detection.

In this paper, we present a novel probabilistic method that addresses these limitations by applying GMM on an MO-based collision detection framework. Rather than explicitly identify system parameters, our approach learns a GMM mapping of the MO residual with respect to system states from the data collected on an excitation trajectory. GMM can represent a wide range of probability distributions due to friction and unmodeled dynamics, and is computationally efficient once the model is trained. This method enables more reliable collision detection without requiring additional sensors.

The key contributions of our work are:

- A data-driven probabilistic framework to improve collision detection accuracy for low-cost manipulators. Its dynamics model is inaccurate. The actuators are controlled by torque commands, but torque or current sensing is not available;
- An implementation of GMM that captures the dynamics from the residual torque of MO, without explicitly identifying model or friction parameters;
- Experimental validation on a custom-made 4-DoF robot manipulator and a comparison with conventional momentum-based collision detection methods. Our method has demonstrated a significant improvement over conventional methods when detecting a mixture of hard and soft collisions, achieving a reduction in the false positive rate by more than 50% at a given true positive rate.

[1]Shao, Singh, Morozovsky, and Yu are with Amazon. Email: {yishao, dbaljees, nickmo, uyupengk} @amazon.com.

[2]Shao is also with the University of Pennsylvania. Email: yishao@seas.upenn.edu. Shao was an intern at Amazon when the work reported in this paper was carried out.

The remainder of this paper is organized as follows: Section II reviews related work in collision detection methods in the presence of model imperfections and sensor restriction. Section III presents our framework and methodology. Section IV describes the experimental setup, results and analysis. And Section V provides a conclusion and future work.

II. RELATED WORK

According to [2], all widely adopted collision monitoring methods use the dynamics model of manipulators to calculate collision monitoring signals. Joint torque measurements, by either torque sensors or motor current sensing, greatly enhance the quality of collision monitoring signals. Among these methods, MO-based collision detection is less sensitive to sensor noise and modeling error because it doesn't require joint acceleration or need to calculate the inverse of the inertia matrix. Therefore, generalized MO has been the standard approach for collision detection in robotics and has been applied widely [6]–[9].

Early implementations of the MO [6], [10] require torque sensors that were expensive. More recent work on the MO demonstrates that if a precise dynamics model of the manipulator and a friction model are available, direct sensing of joint torque is no longer necessary [7]. However, low-cost manipulators are more likely to have imperfections during the fabrication and assembly process. Modeling error of mass, center of mass, inertia, and unmodeled dynamics such as wire harness dynamics will occur. A study in [4] demonstrates that the performance of collision detection with the observer is sensitive to model uncertainties.

Conventional system identification of manipulator dynamic parameters are applied by many research groups [5], [11]–[13] to address the issue of the MO being sensitive to modeling errors. There are a few issues with this approach. First, joint torque sensing is required to accurately identify friction parameters. Second, the excitation trajectory is optimized upon the full regressor matrix, which is computational heavy. Third, not all model parameters are uniquely observable, and manually constraining the parameter range of optimization are needed to ensure reasonable results. Online adaptation of modeling errors is an alternative approach [14], but accurate joint acceleration is necessary to filter out high bandwidth signals from the model adaptation.

In recent years, learning-based approaches to identify system parameters are gaining increasing attention [15]. Popular methods include non-parametric methods such as Gaussian processes [16], [17], and parametric methods such as neural networks [18], [19]. However, pure data-driven methods are computationally expensive [20], while learning of analytical structured forward dynamics suffers from noise on acceleration estimates [15].

In addition to improving model accuracy, many research works aim at directly improving the collision identification performance with an MO. A time-variant threshold for observer residual is proposed in [21], while it introduces several tuning parameters for each joint, and the tuning effort is significant. High-pass filtering the residual is proposed in [22] to separate high-bandwidth dynamics of collisions from low-bandwidth modeling error. However, this article only demonstrates hard collisions, and this method may be limited in identifying soft and light collisions.

Data-driven and learning-based approaches have been applied to MO residual torque, as evidenced by a number of recent research papers. In [23], a multilayer perception neural network is proposed to learn the residual dynamics and construct a semi-parametric model. However, the force estimation accuracy heavily depends on having an accurate dynamics model. In [24], a long short-term memory neural network is trained offline on the manipulator data. Only hard collisions with large magnitude are demonstrated, and the performance degrades significantly in the low-speed region. In [25], different models based on support vector machine and convolutional neural network are proposed. Models are trained to address unknown friction properties on industrial manipulators, while the modeling error is not considered. Methods that use a Gaussian process to improve the MO are proposed in [26], [27]. [26] aims at adapting to bounded modeling error, but it is verified on an industrial robot arm and relies on joint torque measurements. In [27], a Gaussian process framework is proposed to learn residual dynamics. The method aims at improving force estimation performance with modeling errors, but it assumes low-speed manipulator motion with small inertia matrix errors.

GMM is a simple model to cluster data with a finite number of Gaussian distributions [28]. GMM has been widely applied in building cognitive models [29] and controllers [30] for human-robot interaction tasks, due to its versatility. GMMs can represent a wide range of probability distributions and capture complex, non-linear relationships in the data. Once trained, GMMs are computationally efficient for inference, making them suitable for real-time applications. Therefore, GMM has great potential in quantifying uncertainties in the residual torque of the MO.

III. METHODOLOGY

A. Formulation of the Momentum Observer (MO)

Consider an n-DoF robot manipulator with joint positions $q \in \mathbb{R}^n$ and velocities $\dot{q} \in \mathbb{R}^n$. The dynamics are expressed as

$$M(q)\ddot{q} + C(q,\dot{q})\dot{q} + g(q) = \tau_m + \tau_{int} + \tau_{ext} \qquad (1)$$

where $M(q) \in \mathbb{R}^{n\times n}$ is the symmetric and positive-definite inertia matrix, $C(q,\dot{q}) \in \mathbb{R}^{n\times n}$ contains Coriolis and centrifugal terms, $g(q) \in \mathbb{R}^n$ is the gravity vector, $\tau_m \in \mathbb{R}^n$ is the active output torque of each motor, $\tau_{int} \in \mathbb{R}^n$ includes the internal disturbance torque from joint friction and other unmodeled dynamics of the manipulator, and $\tau_{ext} \in \mathbb{R}^n$ represents external torque due to collision.

The external torque $\tau_{ext} \in \mathbb{R}^n$ is estimated based on the generalized MO [2], [6], to avoid explicit calculation of joint accelerations to improve robustness.

Generalized momentum of a manipulator $p \in \mathbb{R}^n$ is written as

$$p = M(q)\dot{q} \qquad (2)$$

The derivative of the generalized momentum is written as

$$\dot{p} = \dot{M}(q)\dot{q} + M(q)\ddot{q} \tag{3}$$

Substituting $\dot{p}$ into the dynamics equation and rearranging terms,

$$\dot{p} = \tau_m + \tau_{int} + \tau_{ext} - C(q,\dot{q})\dot{q} - g(q) + \dot{M}(q)\dot{q} \tag{4}$$

For compactness, we define $\beta(q,\dot{q})$ as the sum of gravity, Coriolis, and inertia variation effects:

$$\beta(q,\dot{q}) = g(q) + C(q,\dot{q})\dot{q} - \dot{M}(q)\dot{q} \tag{5}$$

Note that since $C(q,\dot{q})$ is not uniquely defined, and $\dot{M}(q) - 2C(q,\dot{q})$ is skew-symmetric [31], we have

$$\dot{M}(q) = C(q,\dot{q}) + C^T(q,\dot{q}) \tag{6}$$

Eq. (5) can also be expressed as $\beta(q,\dot{q}) = g(q) + C^T(q,\dot{q})\dot{q}$ to avoid calculating the derivative of the inertia matrix. Since $q, \dot{q}$ and τ_m are measurable, Eq. (4) is estimated as

$$\hat{\dot{p}} = \tau_m - \beta(q,\dot{q}) + r \tag{7}$$

where $r \in \mathbb{R}^n$ is the residual of the MO, which converges to estimated total disturbances $\tau_{int} + \tau_{ext}$. Specifically, if a friction model is available, friction torque τ_f can be included as τ_{int}, and the residual will converge to an estimation of disturbances excluding friction. The residual dynamics is expressed as

$$\dot{r} = K_O(\dot{p} - \hat{\dot{p}}) = K_O(\tau_{int} + \tau_{ext} - r) \tag{8}$$

where K_O is a positive definite observer gain matrix. This results in the residual r converging to the external torque $\tau_{int} + \tau_{ext}$ with first-order dynamics.

The closed form expression of the total residual $r(t)$ in discrete-time domain is expressed as

$$r(t+\Delta t) = K_O\left(p(t) - \sum_{\delta=0}^{t}(\tau_m(\delta) - \beta(q(\delta),\dot{q}(\delta)) + r(\delta)) - p(0)\right) \tag{9}$$

where Δt is the sampling time of the controller.

B. Design of Excitation Trajectory

Prior to collecting data of the residual torque of the MO, the trajectory must be properly designed to sufficiently excite the dynamics across its operational range. A well-designed trajectory ensures that the collected residual torque captures joint friction at a wide range of velocities, modeling error at different arm configurations, and other unmodeled dynamics across its operational range such as flexibility in the links. A popular trajectory proposed in [32] for system identification of manipulator parameters is used in this study, where each joint follows a finite Fourier series. For joint i, the position and velocity profile are written as

$$\begin{aligned} q_i(t) &= q_{i0} + \sum_{k=1}^{N_i} \frac{a_{ik}}{k\omega_f}\sin(k\omega_f t) - \frac{b_{ik}}{k\omega_f}\cos(k\omega_f t) \\ \dot{q}_i(t) &= \sum_{k=1}^{N_i} a_{ik}\cos(k\omega_f t) + b_{ik}\sin(k\omega_f t) \end{aligned} \tag{10}$$

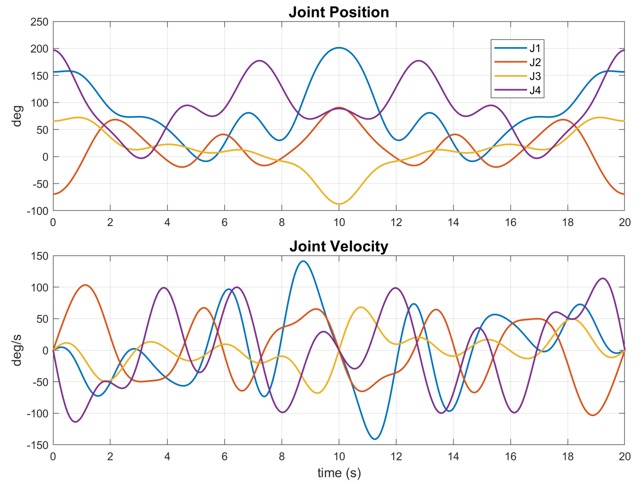

Fig. 1. An example of finite Fourier series trajectories to excite manipulator dynamics for GMM data collection. The starting joint position and velocity are the same as the end position and velocity, so the trajectory can be executed in a loop. The starting joint velocity is 0 to avoid aggressive motions.

where q_{i0} is the initial position offset, N_i is the number of harmonics, $\omega_f = 2\pi/T$ is the fundamental frequency, with T being the period of the trajectory, a_{ik} and b_{ik} are the Fourier coefficients for the k-th harmonic. Values of T and N_i are chosen manually, but they need to be sufficiently large to fully excite system dynamics. The equation of joint acceleration is neglected because precise tracking of joint acceleration is not available on the low-cost manipulator. There is no direct measurement of joint acceleration, and online joint acceleration estimation by double differentiating joint position is noisy due to quantization error.

For each joint, there are a total of $2 \times N_i + 1$ parameters to determine. In typical use cases of system identification, a large scale non-linear optimization problem is formulated, where the objective function is minimizing the condition number of the regressor matrix $\Gamma(q,\dot{q},\ddot{q})$ [33]. The regressor matrix has the same size as the number of data points on the entire trajectory, and minimizing this matrix along the entire trajectory can be computational heavy. As for our application in this study, explicit identification of mechanical parameters is not needed. Instead, all modeling errors and unmodeled dynamics are captured within the torque residual data. Therefore, the regressor matrix condition can be removed from the objective function. Only constraints are added to the trajectory optimization, including joint velocity limit, joint angle limit, and end-effector workspace limit. The $2 \times N_i + 1$ parameters are initialized randomly, and after the optimization returns a solution, the condition number of the regressor matrix is calculated to ensure good but not necessarily optimal excitation of manipulator dynamics. An example of the generated trajectory is shown in Fig. 1.

C. Formulation of the Gaussian Mixture Model (GMM)

A GMM is a probabilistic model that represents a distribution as a weighted sum of Gaussian component densities. GMMs are particularly useful for modeling complex, multimodal distributions and are widely applied in pattern recognition and data clustering. In this paper, data gathered from running the excitation trajectory is collected, and a GMM is trained for each joint. The probability density distribution represents the likelihood of whether the residual torque at a given timestamp is due to the internal dynamics of the manipulator or external disturbances.

The probability density function of a GMM with K components for a D-dimensional data point x is given by

$$\rho(x) = \sum_{k=1}^{K} \pi_k \mathcal{N}(x|\mu_k, \Sigma_k) \tag{11}$$

where K is the number of Gaussian components, π_k are the mixture weights, satisfying $\sum_{k=1}^{K} \pi_k = 1$ and $0 \leq \pi_k \leq 1$, $\mathcal{N}(x|\mu_k, \Sigma_k)$ is the probability density of the k-th Gaussian component with mean vector μ_k and covariance matrix Σ_k.

The Gaussian probability density function for the k-th component is defined as

$$\mathcal{N}(x|\mu_k, \Sigma_k) = \frac{1}{\sqrt{(2\pi)^D |\Sigma_k|}} e^{-\frac{1}{2}(x-\mu_k)^T \Sigma_k^{-1}(x-\mu_k)} \tag{12}$$

In terms of the residual torque collected on a robot manipulator, the main component of internal disturbance is joint friction. The classical friction model can be expressed as

$$\tau_f = f_c \mathrm{sgn}(\dot{q}) + (f_s - f_c)e^{-|v/v_s|}\mathrm{sgn}(\dot{q}) + f_v \dot{q} \tag{13}$$

where f_c is the Coulomb friction coefficient, f_s is the maximum static friction force, v_s is the Stribeck velocity, and f_v is the viscous friction coefficient.

Despite the fact that there are other unmodeled dynamics, we assume the residual torque is closely related to the angular velocity of the corresponding joint. Therefore, a 2-dimensional GMM is constructed from the data of joint angular velocity $\dot{q}_i$, and MO residual r_i which estimates τ_{int} when τ_{ext} is not present. The parameters of a GMM, denoted as $\theta = \{\pi_k, \mu_k, \Sigma_k\}_{k=1}^{K}$, are estimated using the Expectation-Maximization (EM) algorithm [34]. The EM algorithm iteratively refines the parameter estimates to maximize the likelihood of the observed data.

In order to determine the optimal number of Gaussian components K for the GMM on each joint, we employed the Bayesian Information Criterion (BIC). The BIC provides a balance between model complexity and goodness of fit, penalizing overly complex models to prevent overfitting. An "elbow" point on the BIC curve is selected as the optimal value, indicating when the rate of improvement in BIC scores begins to diminish.

D. Online Collision Detection

Once the data of the excitation trajectory are collected and the GMM parameters are estimated, the GMM is implemented online to identify collisions from the residual torque of the MO. For joint i, the probability density of a real-time pair of joint velocity and residual torque, $x_i = [\dot{q}_i, r_i]$, is calculated by Eq. (11). A collision is detected when $\rho([\dot{q}_i, r_i]) < \epsilon$ on any joint, where ϵ is a tunable threshold. This corresponds to a prediction that if there is a low probability of the residual being caused by internal disturbances, there is a high probability that it is caused by external collision.

True Positives (TP) and False Positives (FP) are used to evaluate the collision detection performance. TP is when a collision is happening, and the model successfully detects it; FP happen when the model detects a collision, but a collision is not actually happening. TP rate and FP rate in a collision test are calculated by

$$\text{TP\%} = t_{\text{TP}}/(t_{\text{TP}} + t_{\text{FN}}), \text{FP\%} = t_{\text{FP}}/(t_{\text{FP}} + t_{\text{TN}}) \tag{14}$$

where t_{TP} is the duration of TP, t_{FP} is the duration of FP, t_{FN} is the duration of False Negatives (FN) (when collision is happening but the model doesn't detect it), t_{TN} is the duration of True Negatives (TN) (no collision, and the model doesn't detect a collision).

We compare the collision detection performance of the GMM method with the following baseline methods:

Total residual torque of the MO (TR). Using the total residual torque is the most standard approach to determine whether collision is happening or not. The friction model in Eq. (13) is not included in the equation, and τ_{int} is assumed to be 0. The total residual is compared with a pre-determined and tunable threshold. If the absolute value of the residual is larger, the model raises a collision flag.

Estimated external torque with nominal friction parameters (Nom-f). In many scenarios, joint friction torque can be estimated by a friction model, which is an important part of τ_{int}. If nominal parameters of the classical friction model in Eq. (13) are available, the estimated disturbance can be calculated by $\hat{\tau}_{ext} = r - \tau_{f,nom}$ where $\tau_{f,nom}$ is the nominal friction. The estimated disturbance is then compared with a tunable threshold.

Estimated external torque with identified friction parameters from the excitation trajectory (ID-f). As using GMM is a data-driven approach to cluster unknown dynamic effects shown in the data, in this study we also explicitly identify parameters of the classical friction model from the same datasets with least-squares optimization method. The estimated disturbance can be calculated by $\hat{\tau}_{ext} = r - \tau_{f,id}$ where $\tau_{f,id}$ is the friction torque calculated using identified parameters.

IV. EXPERIMENTAL RESULTS

A. Low-Cost Manipulator Setup

The experiments were conducted on a custom-designed and in-house-fabricated 4-DoF robot manipulator. The links are made of machined aluminum. Each revolute joint is actuated by a brushless DC actuator of the same type. The arm has a total mass of 3.2 kg and a total reach of 0.63 m. Mechanical parameters including mass, inertia of each link and range of motions of joints are from the CAD model of the manipulator, as listed in Table I. In addition, modified Denavit–Hartenberg (D-H) parameters are listed, along with the configuration of the manipulator shown in

TABLE I
PHYSICAL PROPERTIES OF THE 4-DOF MANIPULATOR

Property	**Link1**	**Link2**	**Link3**	**Link4**
Mass (kg)	1.06	1.02	1.00	0.35
Center of Mass (m)	0.003, -0.080, 0.068	0.0, -0.008, 0.063	0.0, -0.013, 0.207	0.0, -0.141, 0.027
Inertia: ($\times 10^{-3}$kg·m²)				
I_{xx}, I_{yy}, I_{zz}	9.0, 4.6, 5.4	3.5, 3.6, 0.8	35.1, 35.1, 0.8	11.2, 0.3, 11.1
I_{yz}, I_{xz}, I_{xy}	3.1, 0.2, 0.2	0.3, 0.0, 0.0	1.3, 0.1, 0.0	0.9, 0.0, 0.0
Property	**Joint1**	**Joint2**	**Joint3**	**Joint4**
Modified D-H Parameters				
a (m)	0.08	0	0	0
α (deg)	0	90	90	-90
d (m)	0	0	0.28	0
θ (deg)	q_1	q_2	q_3	q_4
Angle Limit (deg)	[-100, 150]	[-20, 180]	[-100, 100]	[-120, 120]

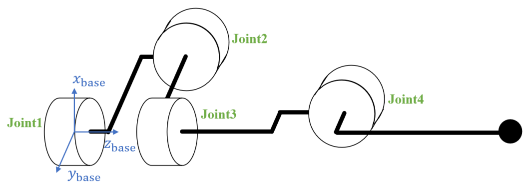

Fig. 2. Configuration of the custom 4-DoF manipulator. Joint 1 is connected to the manipulator base, which is fixed to the tabletop.

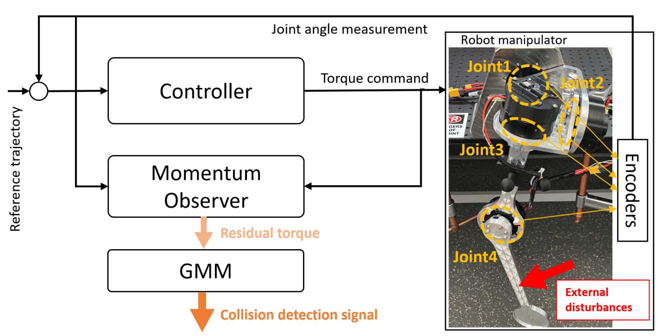

Fig. 3. Controller architecture of using GMM on residual torque of the MO to distinguish external collision from internal torque due to friction, modeling error and unmodeled dynamics.

Fig. 2. Highlights of the mechatronics properties are listed below.

Modeling error. For a low-cost robot manipulator assembled for research or rapid prototyping purposes, there are multiple errors of the mechanical parameters from the CAD model compared to the as-constructed manipulator. The CAD model simplifies features of a motor, ignores details such as screws and nuts, and has variations in material density. In addition, as shown in Fig. 3, power and data cables run outside the arm to avoid constraining joint motions. Mass of the cable and its dragging force while the manipulator is in motion will cause disturbances to the dynamics.

Actuator characteristics. The brushless DC motor comes with a planetary gearbox, and the gear reduction ratio is 10:1. The gearbox magnifies the output torque from the bare motor to the joint by 10 times, while it maintains the backdrivability of the joint. The maximum output torque is 21 Nm. Actuator friction parameters are characterized on a test bench: static friction is 0.52 Nm, Coulomb friction is 0.14 Nm, and viscous friction coefficient is 0.002 Nm/(rad/s). Stribeck effect is not characterized, and we assume the Stribeck velocity is 0.01 rad/s in the nominal friction model. The gearbox also introduces a backlash of 0.1 deg on the output side. However, due to manufacturing tolerances and mechanical wear under work cycles, the actual characteristics of each actuator on the arm can be different from the nominal values.

Sensing availability. Unlike many industrial robot manipulators, the custom manipulator doesn't include a joint torque sensor. An encoder is connected to the input side of each actuator. With the gear reduction, the resolution of measured joint position is 0.1 deg. Joint velocity is obtained by online differentiating joint position at 500 Hz, followed by a low-pass filter with 40 Hz cut-off frequency to reduce noise. Motor current measurement is not available outside the low-level motor controller due to motor firmware limits. Torque commands are converted to current commands before sending to the motor, and the low-level current control loop has a 25 Hz bandwidth. Therefore, we use the torque command as τ_m in Eq. (1), and treat the current loop dynamics as part of τ_{int}. Note that the current command is calculated using a torque constant of 0.94 Nm/A from the datasheet, which is also subject to unit-to-unit variation.

For collision detection experiment, a hand-held 6 DoF force/torque sensor, Robotiq FT 150, is used to measure the external force and torque to the manipulator. This measurement is used as ground truth for analysis only, and it is not streamed to the collision detection module.

Controller implementation. The manipulator software architecture, as shown in Fig. 3, runs on a TI AM69 evaluation board with a ROS 2 environment. An inverse dynamics controller is designed based on the parameters in Table I. The controller along with the collision detection module introduced in this study runs at 500 Hz.

B. Friction Model Identification

An excitation trajectory introduced in Section III-B is implemented. We choose $T = 20$ sec and $N_i = 10$ so that the highest frequency in the Fourier series is $N_i \cdot \omega_f = \pi$ rad/s $=$ 0.5 Hz, which is close to the expected operating condition of our manipulator. Joint angle limits are specified in Table I, and velocity limit is set to 180 deg/s. Many valid trajectories are generated, and an example of what we have implemented on the robot is shown in Fig. 1.

Data of joint velocity and residual torque are collected on each joint. All data points are plotted on a 2-D plot, where the x axis is the joint velocity and the y axis is the residual torque. GMM parameters on each joint are calculated using the EM algorithm, and the probability density distribution is shown in Fig. 4(a). We set the number of GMM components

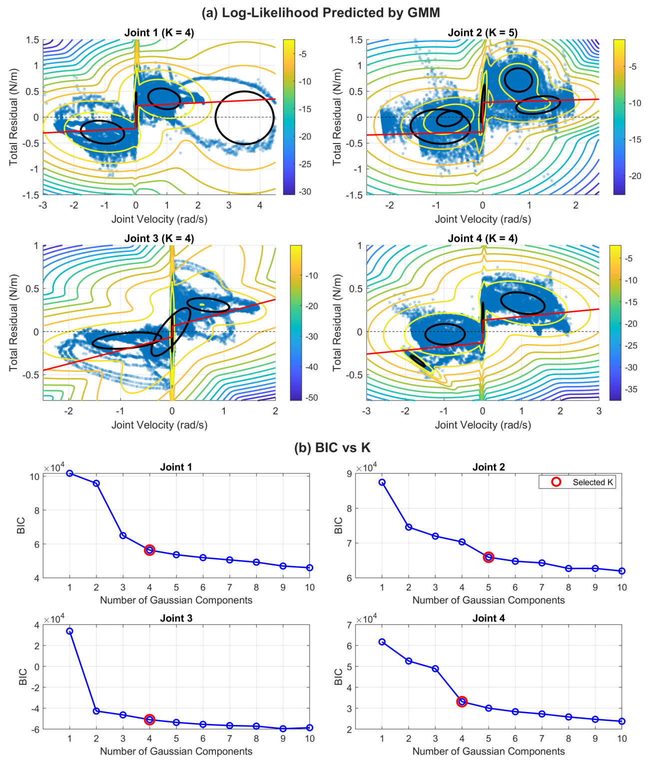

Fig. 4. (a) Negative log-likelihood predicted by GMM on each joint - joint velocity vs. total residual torque of the MO. Blue dots are data points collected on the manipulator while running the excitation trajectory. Black ellipsoids show the mean and covariance of the Gaussian components. Contour lines show the logarithm of the likelihood from high (yellow) to low (blue). Red lines show the classical friction model fitted to the data points. (b) Bayesian Information Criterion (BIC) score vs. number of Gaussian components on each joint.

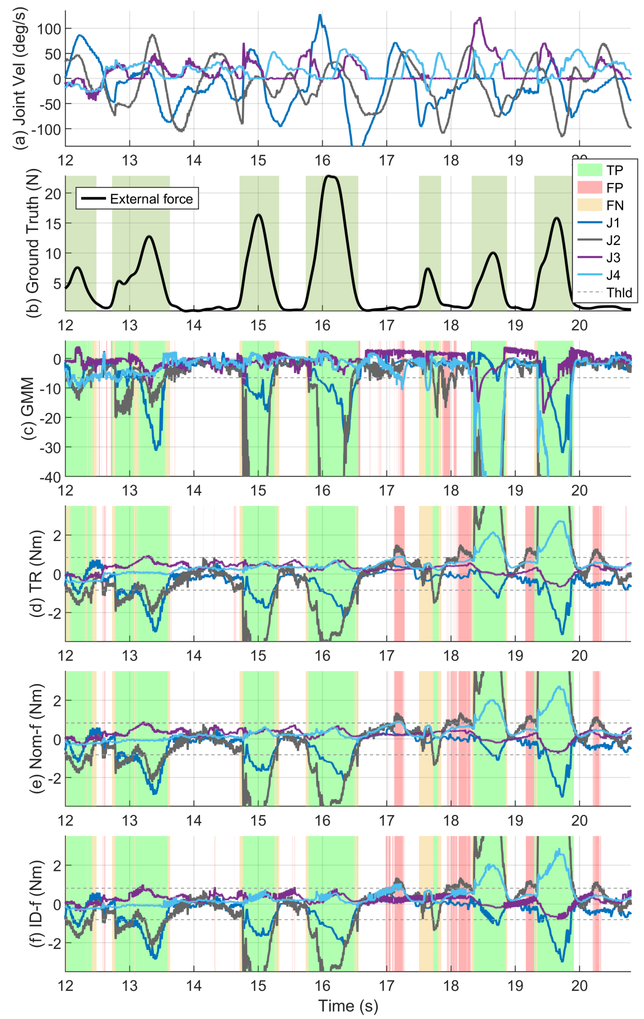

Fig. 5. 8-second detail from a 1-minute collision test result, highlighting True Positive (TP), False Positive (FP), and False Negative (FN) from different methods. Thresholds (Thld) are specified to achieve 90% TP rate for all methods. (a) Joint velocity estimation from encoder measurements. (b) Ground truth collision from hand-held force sensor. (c) GMM method. The scale of y axis is the log-likelihood predicted by the GMM. (d) Total residual method (TR). (e) Nominal friction method (Nom-f). (f) Identified friction parameter method (ID-f).

on each joint to be the elbow point on the curve of the BIC scores vs number of Gaussian components as shown in Fig. 4(b). Note that on Joint 1, large joint velocity appears as tracking error due to an imperfect dynamics model used by the controller, and this effect is captured in one Gaussian component. On Joint 3, although the elbow effect happens when the number of components is 2, more Gaussian components are preferred to capture the complex shape of all data points. GMM fits the dataset without considering the detailed dynamics involving friction, modeling error, or unmodeled dynamics, which makes the modeling process simple and straightforward.

On the other hand, the attempt to identify friction parameters from the data is difficult. Although the data points resemble a profile of friction torque with most data concentrated in the first and the third quadrants, there are some unique features in the data that cannot be explained by friction. At a given joint velocity, the variance of residual torque is large. On Joint 1 and Joint 3, the data show more dynamic behavior, suggesting friction difference between accelerating and decelerating, hysteresis effects, or offsets in one direction of rotation. This can be potentially explained by dynamic friction models such as Dahl or LuGre, but identifying the parameters of such models usually involves complicated data collection process and computationally intensive nonlinear optimizations [35]. In addition, modeling errors of the manipulator dynamics are included in the residual, making friction identification difficult on a low-cost manipulator without a joint torque sensor.

C. Collision Detection Performance

We evaluate collision detection performance using GMM by manually and randomly injecting disturbances to the robot manipulator while it's in motion. To avoid overfitting, the motion trajectory is different from the excitation trajectory: each joint is switching between tracking a fixed-frequency sine wave and rotating at a constant speed. We manually hit the manipulator with the force sensor to replicate the situation of collisions with humans. To demonstrate a general collision scenario, we hit the manipulator at multiple loca-

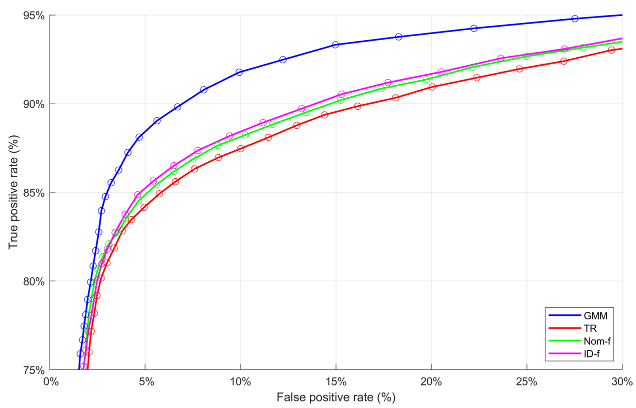

Fig. 6. Comparison of Receiver Operating Characteristics (ROC) curve. TP% $= t_{\text{TP}}/(t_{\text{TP}} + t_{\text{FN}})$, FP% $= t_{\text{FP}}/(t_{\text{FP}} + t_{\text{TN}})$. GMM: GMM method. TR: Total residual method. Nom-f: nominal friction method. ID-f: identified friction parameter method.

tions along each link and at the end-effector. The severity of collision is also varied from low to high magnitude (2 - 20 N), and from short to long duration (0.2 - 4 seconds). Note that some disturbances are not observable to the MO. For example, when the force is parallel to the axis of a revolute joint along the link, the force will not change the momentum. Given this consideration, we focus on evaluating the relative performance of our proposed method against conventional MO-based collision detection methods instead of its absolute TP and FP rates.

Fig. 5 shows the results of a 1-min duration collision test, and the plots are zoomed in for clear visibility of details. The nominal friction parameters are introduced in Section IV-A. The identified friction parameters are shown as the red curves in Fig. 4(a), From the least-squares optimization, the identified static friction coefficient is equal to Coulomb friction coefficient on each joint, and there is no Stribeck effect on the curves. We observe that the GMM method produces less FP than the other methods.

Note that the TP rate and FP rate of a method is largely dependent on the threshold value. A Receiver Operating Characteristics (ROC) graph [36] is used to compare the performance under different threshold settings, as shown in Fig. 6. The ROC graph shows that the GMM method outperforms all the other methods. Relative performance of the GMM method is highest when the targeted TP rate is above 85%. In Fig. 5, the threshold for each method is manually selected from the ROC graph to achieve a same TP rate of 90%. At a 90% TP rate, the FP rate of the GMM method is 7%, where the basic method based on the total residual of the MO has an FP rate of 17%. With a nominal or identified friction model, the performance is improved to 14%, but it is still worse than the GMM method. In summary, GMM provides the lowest FP rate of 7% at a TP rate of 90%.

D. Discussion

Even with the best result demonstrated by the GMM method, a TP rate of 90% and FP rate of 7% may not be acceptable for some scenarios. There are two main reasons. First, performance degradation of the MO is expected on a low-cost manipulator, where there are non-negligible unmodeled dynamics, and joint torque measurement is not available. Second, we intend to evaluate the performance in a generalized situation, where soft and long-duration collisions present together with hard and instant impacts. As shown in Fig. 5, an external force larger than 1.5 N is marked as a disturbance. The effects of noise and unmodeled dynamics are more significant in this case. Therefore, detection of a mixture of hard and soft collisions is challenging for all methods.

In terms of time delay of detection, GMM performs similarly compared with the baseline methods. The reason is that the GMM is applied to the residual torque of the MO, and the observer gain matrix K_o determines the converging rate of the residual torque to the external disturbance. In our experiment, K_o is set to 50 for each joint, resulting in a convergence dynamics bandwidth of 8 Hz, which is more than 10 times higher than the expected operating frequency. The detection time delay, including sensor latency and filtering, is around 50 ms for all methods. The main advantage of the GMM method lies in the TP and FP rates.

Currently, the GMM is set to two dimensions with joint velocity and residual torque. In fact, the residual torque could be dependent on other factors such as axial load or joint position. An advantage of GMM is that it's expandable, and other dimensions can be added easily to incorporate more information to the model.

V. CONCLUSION

This paper presents a novel probabilistic approach to collision detection for low-cost robot manipulators using GMM to capture uncertainties in the residual torque from an MO. Our method addresses the challenges on low-cost manipulators that are not equipped with torque sensors and are subject to modeling errors. GMM is used to cluster residual torque and joint velocity data collected on the manipulator while running a finite Fourier series excitation trajectory. The GMM captures both friction characteristics and unmodeled dynamics without explicit parameter identification. The GMM is then implemented along with the MO to detect collisions in real time. The effectiveness of the proposed framework is demonstrated on a custom-made 4-DoF manipulator by comparing with nominal MO-based collision detection methods with and without friction compensation. At a fixed 90% TP rate in detecting a mixture of hard and soft collisions along the link, the GMM method shows an FP rate of 7% while the FP rates of other methods are 14-17%. This improvement in performance is particularly noteworthy given the hardware limitations and modeling uncertainties inherent in low-cost systems.

For future work, we will investigate improving the performance in realistic manipulation and force interaction tasks. First, Gaussian Model Regression (GMR) can be applied to the residual torque to improve force control by compensating for friction and unmodeled dynamic effects through prediction of GMR. Second, GMM needs to be re-trained due to mechanical wear in work cycles, or modifications to arm configuration such as objects attached to the link. Online adaptation of GMM parameters with real-time data can be developed to capture these slow dynamic changes, eliminating the need for periodic re-training. Third, collision reaction control strategies can be integrated with the collision detection framework to provide an active compliance to enhance safety of physical human-robot interactions.

ACKNOWLEDGMENT

The authors would like to thank Amruta Velapure, Kyle DuFrene, Olga Gomez, and Nicholas Kimball for their assistance with the setup of experiments, Bill Smart, Jong Jin Park and Nathan Kong for their review, and our colleagues at Amazon for their support.

REFERENCES

[1] V. Villani, F. Pini, F. Leali, and C. Secchi, "Survey on human–robot collaboration in industrial settings: Safety, intuitive interfaces and applications," *Mechatronics*, vol. 55, pp. 248–266, 2018.

[2] S. Haddadin, A. De Luca, and A. Albu-Schäffer, "Robot collisions: A survey on detection, isolation, and identification," *IEEE Transactions on Robotics*, vol. 33, no. 6, pp. 1292–1312, 2017.

[3] K. M. Park and F. C. Park, *Collision Detection for Robot Manipulators: Methods and Algorithms*. Springer, 2023.

[4] N. Briquet-Kerestedjian, M. Makarov, M. Grossard, and P. Rodriguez-Ayerbe, "Generalized momentum based-observer for robot impact detection—insights and guidelines under characterized uncertainties," in *2017 IEEE conference on control technology and applications (CCTA)*, pp. 1282–1287, IEEE, 2017.

[5] S. Mamedov and S. Mikhel, "Practical aspects of model-based collision detection," *Frontiers in Robotics and AI*, vol. 7, p. 571574, 2020.

[6] A. De Luca, A. Albu-Schaffer, S. Haddadin, and G. Hirzinger, "Collision detection and safe reaction with the dlr-iii lightweight manipulator arm," in *2006 IEEE/RSJ International Conference on Intelligent Robots and Systems*, pp. 1623–1630, IEEE, 2006.

[7] S.-D. Lee, M.-C. Kim, and J.-B. Song, "Sensorless collision detection for safe human-robot collaboration," in *2015 IEEE/RSJ International Conference on Intelligent Robots and Systems (IROS)*, pp. 2392–2397, IEEE, 2015.

[8] G. Bledt, P. M. Wensing, S. Ingersoll, and S. Kim, "Contact model fusion for event-based locomotion in unstructured terrains," in *2018 IEEE International Conference on Robotics and Automation (ICRA)*, pp. 4399–4406, IEEE, 2018.

[9] V. Morlando, A. Teimoorzadeh, and F. Ruggiero, "Whole-body control with disturbance rejection through a momentum-based observer for quadruped robots," *Mechanism and Machine Theory*, vol. 164, p. 104412, 2021.

[10] S.-D. Lee, Y.-L. Kim, and J.-B. Song, "Novel collision detection index based on joint torque sensors for a redundant manipulator," in *2013 IEEE/RSJ International Conference on Intelligent Robots and Systems*, pp. 4636–4641, IEEE, 2013.

[11] C. D. Sousa and R. Cortesao, "Inertia tensor properties in robot dynamics identification: A linear matrix inequality approach," *IEEE/ASME Transactions on Mechatronics*, vol. 24, no. 1, pp. 406–411, 2019.

[12] Y. Li, Y. Li, M. Zhu, Z. Xu, and D. Mu, "A nonlinear momentum observer for sensorless robot collision detection under model uncertainties," *Mechatronics*, vol. 78, p. 102603, 2021.

[13] L. Pyrhönen, A. Mikkola, and F. Naets, "System identification and force estimation of robotic manipulator using semirecursive multibody formulation," *Multibody System Dynamics*, pp. 1–28, 2024.

[14] S. A. B. Birjandi and S. Haddadin, "Model-adaptive high-speed collision detection for serial-chain robot manipulators," *IEEE Robotics and Automation Letters*, vol. 5, no. 4, pp. 6544–6551, 2020.

[15] A. R. Geist and S. Trimpe, "Structured learning of rigid-body dynamics: A survey and unified view from a robotics perspective," *GAMM-Mitteilungen*, vol. 44, no. 2, p. e202100009, 2021.

[16] C. Della Santina, R. L. Truby, and D. Rus, "Data–driven disturbance observers for estimating external forces on soft robots," *IEEE Robotics and automation letters*, vol. 5, no. 4, pp. 5717–5724, 2020.

[17] G. Giacomuzzo, R. Carli, D. Romeres, and A. Dalla Libera, "A black-box physics-informed estimator based on gaussian process regression for robot inverse dynamics identification," *IEEE Transactions on Robotics*, 2024.

[18] A. Nagabandi, K. Konolige, S. Levine, and V. Kumar, "Deep dynamics models for learning dexterous manipulation," in *Conference on robot learning*, pp. 1101–1112, PMLR, 2020.

[19] C. L. C.-D. De León, S. Vergara-Limón, M. A. D. Vargas-Treviño, J. López-Gómez, J. M. Gonzalez-Calleros, D. M. González-Arriaga, and M. Vargas-Treviño, "Parameter identification of a robot arm manipulator based on a convolutional neural network," *IEEE Access*, vol. 10, pp. 55002–55019, 2022.

[20] O. Sigaud, C. Salaün, and V. Padois, "On-line regression algorithms for learning mechanical models of robots: a survey," *Robotics and Autonomous Systems*, vol. 59, no. 12, pp. 1115–1129, 2011.

[21] V. Sotoudehnejad, A. Takhmar, M. R. Kermani, and I. G. Polushin, "Counteracting modeling errors for sensitive observer-based manipulator collision detection," in *2012 IEEE/RSJ International Conference on Intelligent Robots and Systems*, pp. 4315–4320, IEEE, 2012.

[22] M. Makarov, A. Caldas, M. Grossard, P. Rodriguez-Ayerbe, and D. Dumur, "Adaptive filtering for robust proprioceptive robot impact detection under model uncertainties," *IEEE/ASME Transactions on Mechatronics*, vol. 19, no. 6, pp. 1917–1928, 2014.

[23] J. Hu and R. Xiong, "Contact force estimation for robot manipulator using semiparametric model and disturbance kalman filter," *IEEE Transactions on Industrial Electronics*, vol. 65, no. 4, pp. 3365–3375, 2017.

[24] D. Lim, D. Kim, and J. Park, "Momentum observer-based collision detection using lstm for model uncertainty learning," in *2021 IEEE International Conference on Robotics and Automation (ICRA)*, pp. 4516–4522, IEEE, 2021.

[25] K. M. Park, Y. Park, S. Yoon, and F. C. Park, "Collision detection for robot manipulators using unsupervised anomaly detection algorithms," *IEEE/ASME Transactions on Mechatronics*, vol. 27, no. 5, pp. 2841–2851, 2021.

[26] G. Evangelisti and S. Hirche, "Data-driven momentum observers with physically consistent gaussian processes," *IEEE Transactions on Robotics*, 2024.

[27] Y. Wei, S. Lyu, W. Li, X. Yu, Z. Wang, and L. Guo, "Contact force estimation of robot manipulators with imperfect dynamic model: on gaussian process adaptive disturbance kalman filter," *IEEE Transactions on Automation Science and Engineering*, 2023.

[28] C. M. Bishop and N. M. Nasrabadi, *Pattern recognition and machine learning*, vol. 4. Springer, 2006.

[29] F. Semeraro, A. Griffiths, and A. Cangelosi, "Human–robot collaboration and machine learning: A systematic review of recent research," *Robotics and Computer-Integrated Manufacturing*, vol. 79, p. 102432, 2023.

[30] M. Sharifi, A. Zakerimanesh, J. K. Mehr, A. Torabi, V. K. Mushahwar, and M. Tavakoli, "Impedance variation and learning strategies in human–robot interaction," *IEEE Transactions on Cybernetics*, vol. 52, no. 7, pp. 6462–6475, 2021.

[31] R. M. Murray, Z. Li, and S. S. Sastry, *A mathematical introduction to robotic manipulation*. CRC press, 2017.

[32] J. Swevers, C. Ganseman, D. B. Tukel, J. De Schutter, and H. Van Brussel, "Optimal robot excitation and identification," *IEEE transactions on robotics and automation*, vol. 13, no. 5, pp. 730–740, 1997.

[33] T. Lee, B. D. Lee, and F. C. Park, "Optimal excitation trajectories for mechanical systems identification," *Automatica*, vol. 131, p. 109773, 2021.

[34] D. Chen, G. Li, D. Zhou, and Z. Ju, "A novel curved gaussian mixture model and its application in motion skill encoding," in *2021 IEEE/RSJ International Conference on Intelligent Robots and Systems (IROS)*, pp. 7813–7818, IEEE, 2021.

[35] S. Mahmoudkhani, J. Gorenstein, and K. Ahmadi, "A new iterative identification algorithm for estimating the lugre friction model parameters," *Mechanism and Machine Theory*, vol. 203, p. 105797, 2024.

[36] T. Fawcett, "An introduction to roc analysis," *Pattern recognition letters*, vol. 27, no. 8, pp. 861–874, 2006.